ACS Catalysis

Research Article

pubs.acs.org/acscatalysis

Platinum-Coated Palladium Nanotubes as Oxygen Reduction Reaction Electrocatalysts

Shaun M. Alia,[†,§] Kurt O. Jensen,[†,§] Bryan S. Pivovar,[‡] and Yushan Yan*[,†,§]

[†]Department of Chemical Engineering, University of Delaware, Newark, Delaware 19716, United States

[§]Department of Chemical and Environmental Engineering, University of California, Riverside, California 92521, United States

[‡]National Renewable Energy Laboratory, Golden, Colorado 80401, United States

Supporting Information

ABSTRACT: Platinum (Pt) coated palladium (Pd) nanotubes (Pt/PdNTs) with a wall thickness of 6 nm, outer diameter of 60 nm, and length of 5−20 μm are synthesized via the partial galvanic displacement of Pd nanotubes. Pt coatings are controlled to a loading of 9 (PtPd 9), 14 (PtPd 14), and 18 (PtPd 18) wt % and estimated to have a thickness of 1.1, 1.7, and 2.2 Pt atoms, respectively, if a uniform and continuous coating is assumed. Oxygen reduction experiments have been used to evaluate Pt/PdNTs, Pt nanotubes, Pd nanotubes, and supported Pt nanoparticle activity for proton exchange membrane fuel cell cathodes. The dollar and area (specific surface area) normalized ORR activities of Pt/PdNTs exceed the United States Department of Energy (DOE) targets. PtPd 9, PtPd 14, and PtPd 18 produce dollar activities of 10.4, 9.4, and 8.7 A^{-1}, respectively; PtPd 9 exceeds the DOE dollar activity target (9.7 A^{-1}) by 7%. Pt/PdNTs further exceed the DOE area activity target by 40−43%.

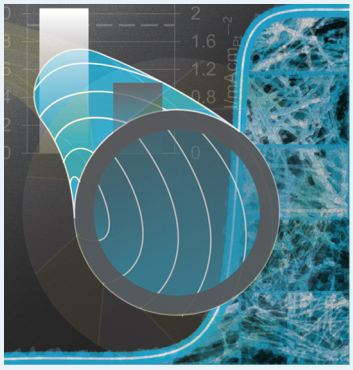

KEYWORDS: *proton exchange membrane fuel cells, platinum nanotubes, core shell catalysts*

INTRODUCTION

Proton exchange membrane fuel cells (PEMFCs) can have high power densities and zero emissions. Commercialization of this technology, however, is primarily limited by high catalyst cost.[1] The development of highly active cathode catalysts is of particular interest since the overpotential for the oxygen reduction reaction (ORR) is significantly larger than the hydrogen oxidation reaction.[2,3] Platinum (Pt) nanoparticles supported on carbon (Pt/C) is commonly used as an ORR catalyst; the low specific surface area activity (subsequently referred to as area activity) of Pt/C, however, hampers PEMFC deployment.[4,5] To promote the development of Pt catalysts with high ORR activity, the United States Department of Energy (DOE) set targets (2010−2015) for mass activity (0.44 Amg^{-1}) and area activity (0.72 mAcm^{-2}) on a Pt basis.

Studies have been completed on Pt coatings and Pt alloys in an effort to reduce catalyst cost and increase activity.[6] Since these materials contain non-Pt components, normalizing activities to the Pt mass does not adequately account for the cost of the alloy or support. While this study includes activities normalized to the total metal and Pt mass, a dollar activity is introduced to objectively quantify the cost of this class of catalyst. Dollar activities are calculated as a mass activity normalized to metal price derived from the 5 year average (July 2006−July 2011) metal prices of Pt ($ 1414. 68 t oz^{-1}, $ 45.48 g^{-1}) and palladium (Pd) ($ 392.95 t oz^{-1}, $ 12.63 g^{-1}). The DOE mass activity target (0.44 Amg$_{Pt}^{-1}$) corresponded to a dollar activity of 9.7 A^{-1}.

Pt alloys and coatings have previously been studied for ORR activity.[7−12] Nørskov et al. examined polycrystalline Pt films alloyed with nickel (Ni), cobalt (Co), iron (Fe), vanadium, and titanium, and showed that the ORR area activity of the Pt_3Co film was three times greater than pure Pt.[8] Stamenkovic et al. and Sun et al. examined PtFe nanoparticles for ORR; Stamenkovic et al. was able to produce Pt_3Fe nanoparticles with a 3-fold improvement in Pt mass activity to Pt nanoparticles.[9,10] Stamenkovic et al. and Fang et al. further studied PtNi based catalysts, exceeding the DOE Pt mass and area activity targets for ORR.[11,12] Although Pt metal alloys have shown improved ORR activity, these transition metals have a low redox potential (Co −0.28 V, Fe −0.44 V, and Ni −0.25 V) and their dissolution during PEMFC operation remains a significant concern.[6] In Pt coatings, Adzic et al. electrochemically coated Pd with a monolayer of Pt; although Pt-coated Pd had a higher ORR activity than pure Pt, electrochemical deposition faces concerns for large scale synthesis.[7] The synthesis of PtPd catalysts was also studied previously by Xia et al. in the form of nanodendrites.[13] Although PtPd nanodendrites had a high surface area (48.5 m^2 g$_M^{-1}$), the ORR area activity (0.42 mA cm$_M^{-2}$) was below the DOE target; furthermore the Pt content (85 wt %) was too high to meet the

Special Issue: Electrocatalysis

Received: December 22, 2011
Revised: April 4, 2012
Published: April 6, 2012

dollar activity target (5.0 A $\$^{-1}$). The bulk synthesis of Pt-coated Pd is desirable due to the moderate ORR activity of Pd and the reduced cost of the Pd substrate. The use of the metal substrate (as opposed to an insulating substrate) further ensures complete utilization of the Pt shell.

Previously, PtNTs and PtPd alloyed nanotubes were examined as ORR catalysts; the extended surface and electronic and lattice tuning produced an area activity significantly larger than conventional nanoparticles.[14,15] PtNTs were found to produce a dollar activity of 3.75 A$\$^{-1}$; to meet the DOE dollar activity target in a PtPd nanotube, the Pt content had to be reduced to 15 wt % assuming constant area activity and surface area. To meet this target, Pd nanotubes (PdNTs) were coated with Pt by partial galvanic displacement, forming Pt-coated PdNTs (Pt/PdNTs). PdNTs were partially displaced with Pt presumably resulting in a continuous Pt layer on the surface, reducing catalyst cost while maintaining ORR activity. This study is the first to coat atomic sized layers of Pt onto a Pd substrate without the aid of actively controlled electrochemical deposition.

EXPERIMENTAL SECTION

Silver (Ag) nanowires (AgNWs) were synthesized via the reduction of Ag nitrate with ethylene glycol in the presence of chloroplatinic acid, provided for wire seeding, and polyvinyl pyrollidone, provided for morphological control.[16,17] PtNTs and PdNTs were synthesized by the galvanic displacement of AgNWs.[17,18] Pt/PdNTs were synthesized by the partial galvanic displacement of PdNTs with Pt.

Ethylene glycol was refluxed at approximately 197.3 °C over 4 h in the presence of argon prior to AgNW synthesis to ensure the removal of trace amounts of alcohol. For AgNW synthesis, 15 mL of ethylene glycol was heated to 170 °C in a 3-neck round-bottom flask equipped with a thermocouple, condenser passing argon, addition funnel, and stir bar. After 10 min at 170 °C, a 1.25 mL solution of chloroplatinic acid in ethylene glycol (0.4 mM) was injected. Following a 5 min wait period, 18 mL of 0.1 M polyvinyl pyrollidone (molecular weight 40 000) and 0.05 M silver nitrate in ethylene glycol was added to the flask dropwise over 19 min via the addition funnel. The reaction was allowed to continue for 5 min, at which point the flask was immersed in an ice bath. AgNWs (5 mL aliquots) were distributed into 50 mL centrifuge tubes and washed in ethanol, acetone, and water. The AgNW synthesis procedure utilized was largely consistent with those previously published; a slightly higher temperature was utilized, however, as this method reduced particle content prior to nanowire cleaning.[16,17]

In PtNT synthesis, 20 mL of cleaned AgNWs (75.5 mg) were dispersed in 200 mL of water saturated with sodium chloride. The solution was added to a 500 mL 3-neck round-bottom flask equipped with a thermocouple, condenser passing argon, stir bar, and an addition funnel containing 100 mL of 0.86 mM chloroplatinic acid. Following 15 min at reflux at approximately 108.7 °C, the chloroplatinic acid solution was added dropwise to the flask over a period of 15 min. The flask then proceeded at reflux (108.7 °C) for 1 h before the reaction was quenched in an ice bath. The flask contents were subsequently washed with a saturated sodium chloride solution and water. PdNTs were synthesized by dispersing 75.5 mg of AgNWs in 400 mL of a 16.7 mM polyvinyl pyrollidone in water solution saturated with sodium chloride. The solution was added to an experimental apparatus identical to PtNT synthesis, with the addition funnel containing 200 mL of 1.8 mM sodium tetrachloropalladate. Reaction and cleaning protocols were identical to the PtNT synthesis. The PtNT and PdNT synthesis procedures were similar to those previously published.[17,18] This method deviated in synthesis temperature (108.7 °C), as the increase reduced nanotube surface roughness. PdNTs were synthesized with a sodium tetrachloropalladate precursor to ensure that Ag displacement yielded Ag chloride, thereby increasing the favorability of the Pd−Ag displacement reaction. Polyvinyl pyrollidone (molecular weight 40 000) was also added during PdNT synthesis to aid in the cleaning process.

Pt/PdNTs were synthesized by adding PdNTs (51.1 mg) to 400 mL of water in a 1-L 3-neck round-bottom flask containing a thermocouple, condenser passing argon, stir bar, and addition funnel containing 200 mL of chloroplatinic acid (8.5 mg for 9 wt %, 12.2 mg for 14 wt %, 15.6 mg for 18 wt %). Although small amounts of Pt were added, the addition funnel volume was identical to the PtNT and PdNT syntheses (200 mL); in the synthesis of Pt/PdNTs, a lower chloroplatinic acid concentration was vital in slowing the displacement reaction and forming a Pt shell.[19] Reaction and cleaning protocols were identical to the PtNT synthesis.

Prior to electrochemical testing, PtNTs, PdNTs, and Pt/PdNTs were washed with 0.5 M HNO_3 in an argon environment for 2 h to ensure the removal of any remaining Ag. PtNTs and PdNTs were subsequently annealed at 250 °C in a forming gas environment (5% hydrogen, balance nitrogen). Pt/PdNTs were annealed at 150 °C to prevent migration of surface Pt into the Pd substrate. The exposure of Pt/PdNTs to elevated temperatures (>200 °C) reduced ORR performance to an activity comparable to PdNTs; it was anticipated that temperature exacerbated alloying and increased the driving force for Pd to exist on the nanotube surface.[19]

Scanning electron microscopy (SEM) images were taken at 20 kV using a Philips XL30-FEG microscope. Transmission electron microscopy (TEM) images were taken at 300 kV using a Philips CM300 microscope with samples pipetted onto a holey carbon coatings supported on copper grids. Selected area electron diffraction (SAED) patterns were taken at a length of 24.5 and 32.0 cm. Electrochemical experiments were completed with a multichannel potentiostat (Princeton Applied Research) and a Modulated Speed Rotator equipped with a 5 mm glassy carbon electrode (Pine Instruments). Rotating disk electrode (RDE) experiments were conducted in a three-electrode cell, with a glassy carbon electrode, platinum wire, and double junction silver/silver chloride electrode (Pine Instruments) utilized as the working, counter, and reference electrodes, respectively.

Catalysts were dispersed in 2-propanol to form a dilute suspension (0.784 mg mL^{-1}); a thin catalyst layer was formed on the RDE working electrode by pipetting the catalyst suspension to a loading of 40 $\mu g\ cm^{-2}$ (10 μL). The catalyst layer thickness was approximately 54 nm, calculated assuming the nanotubes aligned in a honeycomb stack and accounting for nanotube curvature. Following catalyst addition, the working electrode dried in air at room temperature; 10 μL of 0.05 wt % Nafion (Liquion) was subsequently pipetted onto the working electrode to ensure adhesion and protect the catalyst layer during rotation.

ORR and cyclic voltammetry experiments were completed at a scan rate of 20 mVs^{-1} in a 0.1 M $HClO_4$ electrolyte.[20,21] Area normalized activities were calculated with electrochemically

dx.doi.org/10.1021/cs200682c | ACS Catal. 2012, 2, 858−863

active surface areas (ECSAs) as determined by carbon monoxide oxidation. Conversions between the Ag/AgCl reference electrode and a reversible hydrogen electrode (RHE) were conducted by measuring the potential drop between the reference electrode and a bulk polycrystalline Pt (BPPt) electrode in a hydrogen-saturated electrolyte.[22] Electrode potentials were corrected for internal resistance during oxygen reduction experiments by impedance spectroscopy measurements taken between 10 kHz and 0.1 mHz. Approximate steady state conditions were ensured by measuring RHE values prior to and following electrochemical testing.

RESULTS AND DISCUSSION

Pt/PdNTs were synthesized with Pt loadings of 9 wt % (PtPd 9), 14 wt % (PtPd 14), and 18 wt % (PtPd 18) of the total catalyst mass (Figure 1c–h). PdNTs and PtNTs were also included as benchmarks to aid in catalyst evaluation (Figure 1a–b and i–j). Pt/PdNTs and PdNTs had a wall thickness of 6 nm, an outer diameter of 60 nm, and a length of 5–20 μm; conversely, PtNTs had a wall thickness of 5 nm (Supporting Information Figure S.2–S.4). The AgNW template was synthesized with a 60 nm diameter and a length of 10–500 μm (Supporting Information Figure S.1). Pt content within the Pt/PdNTs was determined by energy dispersive X-ray spectroscopy (EDS). A high degree of surface roughness was observed on the Pt/PdNTs, attributed to the PdNT template (Figure 1 and Supporting Information Figure S.2); since the size and frequency of surface nodules was identical between the Pt/PdNTs and PdNTs, it was concluded that the rough surface formed during PdNT synthesis, not the Pt coating process.

TEM images confirmed that the nanotubes consisted of nanoparticles. Alignment of the nanoparticles within the nanotubes was confirmed with SAED patterns, which displayed the superimposed [001] and [1,−1,−2] zones, with reflections of {100} ([001] zone), {111} ([1,−1,−2] zone), and {110} ([001] and [1,−1,−2] zones) present. SAED patterns confirmed common growth directions among the PdNTs, PtPd 9, and PtNTs. High resolution TEM images were utilized in examining the (1,1,−1) lattice spacings; it was anticipated that the fcc crystallographic structure and similar atomic size of Pt, Pd, and Ag contributed to the templated growth directions and lattice spacing.

Catalyst ECSAs were determined by carbon monoxide oxidation voltammograms (Figure 2).[23] A monolayer of carbon monoxide was adsorbed onto the catalyst surface by holding a potential of 0.2 V vs RHE for 10 min in a carbon monoxide (10% carbon monoxide, balance nitrogen) saturated electrolyte. A potential of 0.2 V vs RHE was utilized to prevent hydrogen adsorption on Pt/PdNTs and PdNTs. Prior to voltammograms, the catalyst was held at 0.2 V vs RHE for 10 min under argon to fully remove excess carbon monoxide in the electrolyte. The ECSAs of PdNTs, PtPd 9, PtPd 14, PtPd 18, PtNTs, and Pt/C were 16.2, 16.0, 15.7, 15.9, 16.3, and 64.0 $m^2\ g^{-1}$. ECSAs were determined assuming a Coulombic charge of 420 $\mu C\ cm^{-2}$ and were utilized in ORR area activity calculations. These calculations were further verified with the charge associated with hydrogen adsorption; for PdNTs and Pt/PdNTs, charge associated with hydrogen evolution near 0.05 V vs RHE was not included in the ECSA calculation (Supporting Information Figure S.5).

The ORR activity of PdNTs, Pt/PdNTs, PtNTs, Pt/C, and BPPt was evaluated with RDE experiments (Figure 3). Kinetic

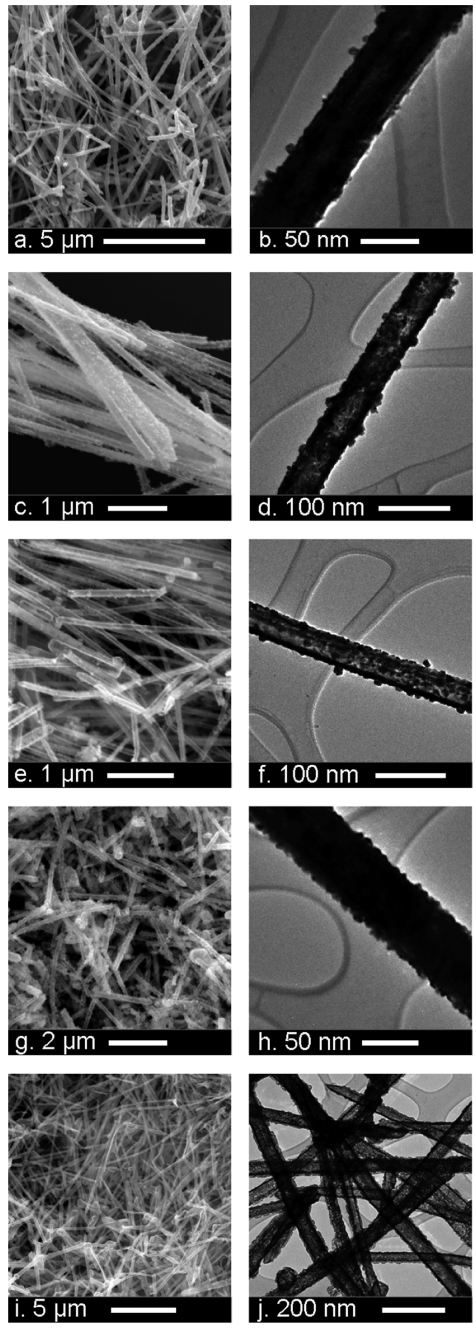

Figure 1. SEM and TEM images of (a–b) PdNTs, (c–d) PtPd 9, (e–f) PtPd 14, (g–h) PtPd 18, and (i–j) PtNTs.

activities were determined at 0.9 V vs RHE during anodic polarization scans at 1600 rpm and a scan rate of 20 mV s^{-1}. Catalyst activity for ORR was assessed in terms of total metal mass (M), Pt mass (Pt), dollar, and area (Figure 4 and Supporting Information Figure S.6). Pt/PdNTs maintained metal mass activities 94–95% of PtNTs; similarly, Pt/PdNTs produced area activities 96–98% of PtNTs. The Pt/PdNTs exceeded the area activities of the DOE target by 40–43%. Because of the reduction in Pt loading, the Pt mass activity of Pt/PdNTs was significantly higher than PtNTs. PtPd 9 produced a Pt mass activity of 1.8 A mg_{Pt}^{-1}, exceeding a Pt DOE target by approximately 4-fold. Furthermore, the dollar activity of PtPd 9 was 10.4 A $\$^{-1}$, exceeding the DOE target by 7%. PtPd 14 and PtPd 18 produced 97% and 90% of the target

dx.doi.org/10.1021/cs200682c | ACS Catal. 2012, 2, 858–863

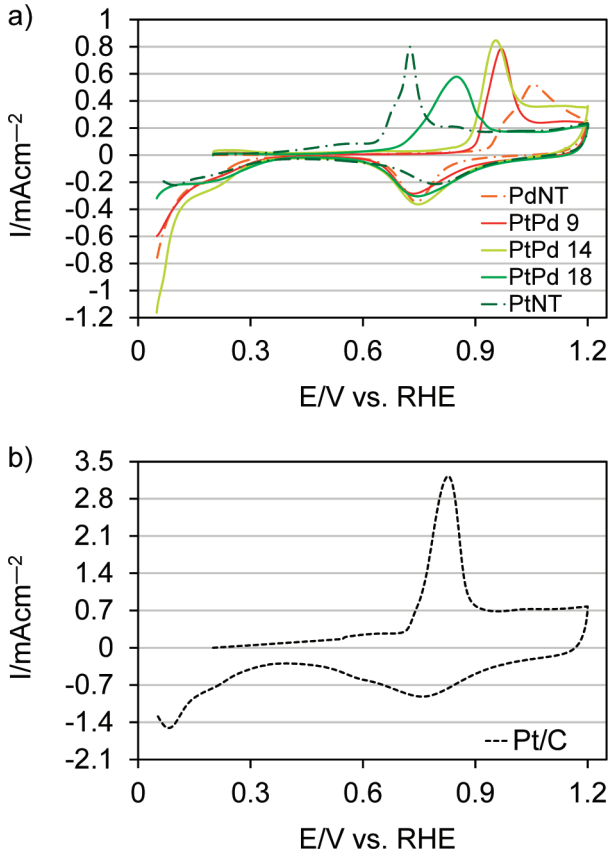

Figure 2. Carbon monoxide oxidation voltammograms of (a) PtPd 9, PtPd 14, PtPd 18, PtNTs, and PdNTs and (b) Pt/C at 20 mV s^{-1} in a carbon monoxide saturated 0.1 M HClO4 electrolyte.

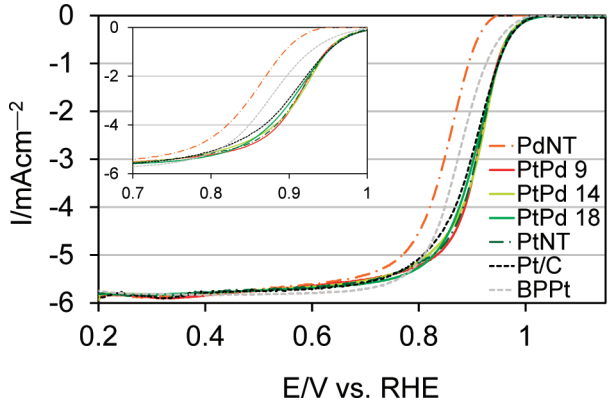

Figure 3. Anodic polarization scans of PtPd 9, PtPd 14, PtPd 18, PtNTs, PdNTs, Pt/C, and BPPt in an oxygen saturated 0.1 M $HClO_4$ electrolyte. Data was collected at a scan rate of 20 mV s^{-1} and a rotation speed of 1600 rpm.

value, but each of the Pt/PdNTs dramatically exceeded the dollar activity of Pt/C (2.5−3.0 times).

Catalyst activity for ORR was also evaluated in terms of area per dollar (Figure 5). The DOE dollar activity target (9.67 A $\$^{-1}$) was represented by the solid line, indicating the area activity required to exceed the DOE target at a given area per dollar; activities to the upper right of the solid line signify an ORR activity in excess of this value. Although Pt/C expressed the largest area per dollar (1.4 m^2 $\$^{-1}$), the area activity was inadequate to approach the dollar activity target. While PtNTs

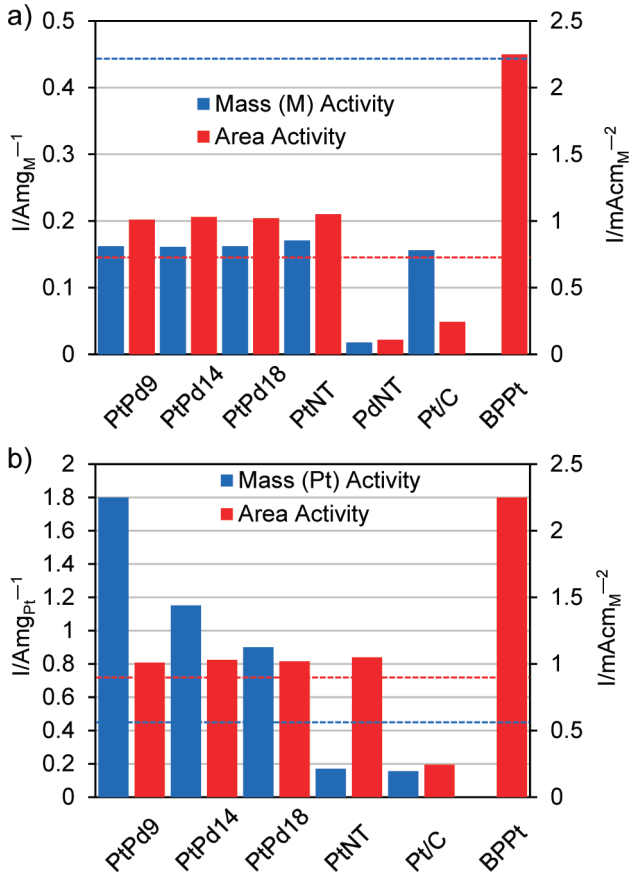

Figure 4. (a) Activity normalized to total metal mass and area and (b) activity normalized to Pt mass and area of PtPd 9, PtPd 14, PtPd 18, PtNTs, PdNTs, Pt/C and BPPt; DOE targets are denoted by dotted lines (···).Catalyst activities were determined at 0.9 V vs RHE during anodic polarization scans at 1600 rpm and 20 mV s^{-1} in a 0.1 M $HClO_4$ electrolyte.

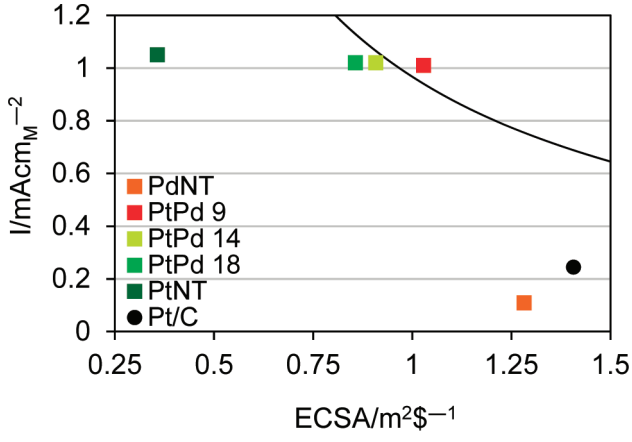

Figure 5. Area activity as a function of cost normalized surface area; DOE mass activity target denoted by a solid line (—). Catalyst activities were determined at 0.9 V vs RHE during anodic polarization scans at 1600 rpm and 20 mV s^{-1} in a 0.1 M $HClO_4$ electrolyte.

produced a much larger area activity, the area per dollar (0.4 m^2 $\$^{-1}$) was far too low. For Pt/PdNT catalysts, the area per dollar increased as the Pt loading dropped. PtPd 9 expressed an area per dollar of 1.0 m^2 $\$^{-1}$, thereby exceeding the DOE dollar activity target.

dx.doi.org/10.1021/cs200682c | ACS Catal. 2012, 2, 858−863

Catalyst ORR activity was further examined in tafel and turnover frequency (TOF) plots. The tafel slopes of Pt/PdNTs and PtNTs were smaller than Pt/C in both the low and high current density regions; the tafel slopes of Pt/C and BPPt were similar to values previously reported (Supporting Information Figure S.7 and Table S.1).[24,25] Furthermore, the TOFs of Pt/PdNTs were 3-fold to 4-fold higher than Pt/C in the low current density region (Supporting Information Figure S.8)

Presence of a Pt−Pd shell−core structure was confirmed with ORR area activities and carbon monoxide oxidation voltammograms. With a uniform coating of Pt, a wall thickness of 6 nm, and a {100} lattice spacing of 2.5 Å, the Pt loadings of 9 wt %, 14 wt %, and 18 wt % corresponded to a theoretical coating of 1.1, 1.7, and 2.2 Pt atoms. The Pd substrate could have potentially affected the ORR activity of Pt/PdNTs by modifying: the Pt facets expressed on the nanotube surface; the shell lattice spacing; the shell d-band filling; or the catalysts' oxygen adsorption characteristics.[7,8,26] HRTEM images and SAED diffraction patterns confirmed identical growth directions and similar lattice spacings of the nanotube catalysts (Supporting Information Figure S2−S4). Furthermore, Pt and Pd have similar O and OH binding energies and the calculated d-band center shift for a Pt overlayer on Pd was minimal.[27,28] Although the Pd substrate modified the oxygen adsorption profile of Pt/PdNTs, the potential for metal oxidation was largely the same for Pt and Pd catalysts; anodic polarization scans further reduced the influence of hysteresis during ORR experiments (Supporting Information Figure S.9). The Pd substrate, therefore, was expected to have a slight effect on the ORR activity of the Pt shell. Although electronic tuning could have influenced ORR activity, the lower area activity of Pt/PdNTs could also have been caused by Pd impurities in the shell. PtPd 9, PtPd 14, and PtPd 18 produced ORR area activities 2.9, 1.9, and 3.8% lower than PtNTs.

Carbon monoxide oxidation voltammograms further confirmed a thickening of the Pt shell as the Pt loading increased (Figure 2).[29] Previously, Eichhorn and Mavrikakis et al. and Sunde et al. confirmed the presence of Pt−Ru shell−core nanoparticles by the lack of multiple carbon monoxide oxidation peaks; repeated oxidation experiments induced the dissolution of surface Ru, thereby determining if the original shell was pure Pt.[30,31] Since the fast dissolution of Pd was impractical, the location of the carbon monoxide oxidation peaks was used to confirm the Pt coating. Differences in Pt and Pd carbon monoxide oxidation potentials were attributed to the ability of the transition metals to back-donate d electrons to carbon monoxide during chemisorption, thereby weakening the carbon/oxygen bond.[32] PtNTs and PdNTs produced carbon monoxide oxidation peaks at potentials of 0.7 and 1.0 V, respectively. PtPd 9 and PtPd 14 produced a peak at approximately 0.95 V, indicating Pt bound to subsurface Pd (Pt−Pd). The shift in peak position of Pt−Pd (0.95 V) was attributed to the presence of a Pt surface tuned by the Pd substrate. The presence of one carbon monoxide oxidation peak confirmed surface uniformity and indicated the formation of a continuous Pt layer rather than Pt particles. For PtPd 18, the carbon monoxide oxidation peak shifted to approximately 0.85 V. This shift was attributed to a thickening of the Pt shell and the increased prevalence of Pt bound to subsurface Pt (Pt−Pt). In this manner, it appeared likely that increased Pt loadings uniformly increased the Pt shell thickness.

CONCLUSIONS

In summary, the work presented here demonstrates that nanotube templated Pt coatings are clearly the path for the development of PEMFC cathode catalysts. The Pt content of pure PtNTs was decreased to 9 wt %, replacing nearly all subsurface Pt with Pd; PtPd 9 produced an ORR mass activity 95% of PtNTs. The dollar activity of PtPd 9, therefore, was 2.8 times greater and exceeded the DOE target. The area activity of Pt/PdNTs further matched PtNTs and outperformed the DOE target by greater than 40%. Similar to PtNTs, it is anticipated that Pt/PdNTs would allow for a thin electrode catalyst layer because of the absence of a low density carbon support, improving Pt utilization and mass transport. The solution based synthesis of sub nanometer templated coatings is a milestone in its own right and pertinent to a variety of applications for nanomaterial electrocatalysts.

ASSOCIATED CONTENT

Supporting Information

Figures and tables showing further catalyst characterization and price analysis. The catalyst characterization section includes structural data (SEM, TEM, SAED) and electrochemical results: cyclic voltammograms; ORR activity; Tafel plots and slopes; and TOF plots. The price analysis section includes: metal prices; metal demands; and a price elasticity table. This material is available free of charge via the Internet at http://pubs.acs.org.

AUTHOR INFORMATION

Corresponding Author

*Fax: 302.831.2582. E-mail: yanys@udel.edu.

Notes

The authors declare no competing financial interest.

ACKNOWLEDGMENTS

This work was supported by the U.S. Department of Energy through the Fuel Cell Technologies Program under Contract No. DE-AC36-08-GO28308 with the National Renewable Energy Laboratory.

REFERENCES

(1) Gasteiger, H. A.; Kocha, S. S.; Sompalli, B.; Wagner, F. T. *Appl. Catal., B* **2005**, *56*, 9−35.
(2) Markovic, N. M.; Grgur, B. N.; Ross, P. N. *J. Phys. Chem. B* **1997**, *101*, 5405−5413.
(3) Paulus, U. A.; Schmidt, T. J.; Gasteiger, H. A.; Behm, R. J. *J. Electroanal. Chem.* **2001**, *495*, 134−145.
(4) Bregoli, L. J. *Electrochim. Acta* **1978**, *23*, 489−492.
(5) Kinoshita, K. *J. Electrochem. Soc.* **1990**, *137*, 845−848.
(6) Bing, Y. H.; Liu, H. S.; Zhang, L.; Ghosh, D.; Zhang, J. J. *Chem Soc Rev* **2010**, *39*, 2184−2202.
(7) Zhang, J.; Mo, Y.; Vukmirovic, M. B.; Klie, R.; Sasaki, K.; Adzic, R. R. *J. Phys. Chem. B* **2004**, *108*, 10955−10964.
(8) Stamenkovic, V.; Mun, B. S.; Mayrhofer, K. J. J.; Ross, P. N.; Markovic, N. M.; Rossmeisl, J.; Greeley, J.; Nørskov, J. K. *Angew. Chem.* **2006**, *118*, 2963−2967.
(9) Wang, C.; van der Vliet, D.; More, K. L.; Zaluzec, N. J.; Peng, S.; Sun, S. H.; Daimon, H.; Wang, G. F.; Greeley, J.; Pearson, J.; Paulikas, A. P.; Karapetrov, G.; Strmcnik, D.; Markovic, N. M.; Stamenkovic, V. R. *Nano Lett* **2011**, *11*, 919−926.
(10) Guo, S.; Sun, S. *J. Am. Chem. Soc.* **2012**, *134*, 2492−2495.
(11) van der Vliet, D.; Wang, C.; Debe, M.; Atanasoski, R.; Markovic, N. M.; Stamenkovic, V. R. *Electrochim. Acta* **2011**, *56*, 8695−8699.

(12) Yang, H. Z.; Zhang, J.; Kumar, S.; Zhang, H. J.; Yang, R. D.; Fang, J. Y.; Zou, S. Z. *Electrochem. Commun.* **2009**, *11*, 2278−2281.
(13) Xia, Y. A.; Lim, B.; Jiang, M. J.; Camargo, P. H. C.; Cho, E. C.; Tao, J.; Lu, X. M.; Zhu, Y. M. *Science* **2009**, *324*, 1302−1305.
(14) Alia, S. M.; Zhang, G.; Kisailus, D.; Li, D. S.; Gu, S.; Jensen, K.; Yan, Y. S. *Adv. Funct. Mater.* **2010**, *20*, 3742−3746.
(15) Chen, Z. W.; Waje, M.; Li, W. Z.; Yan, Y. S. *Angew. Chem., Int. Ed.* **2007**, *46*, 4060−4063.
(16) Sun, Y. G.; Yin, Y. D.; Mayers, B. T.; Herricks, T.; Xia, Y. N. *Chem. Mater.* **2002**, *14*, 4736−4745.
(17) Chen, J. Y.; Wiley, B. J.; Xia, Y. N. *Langmuir* **2007**, *23*, 4120−4129.
(18) Sun, Y. G.; Mayers, B.; Xia, Y. N. *Adv. Mater.* **2003**, *15*, 641−646.
(19) Ruban, A. V.; Skriver, H. L.; oslash; rskov, J. K. *Phys. Rev. B* **1999**, *59*, 15990.
(20) Takahashi, I.; Kocha, S. S. *J. Power Sources* **2010**, *195*, 6312−6322.
(21) Garsany, Y.; Baturina, O. A.; Swider-Lyons, K. E.; Kocha, S. S. *Anal. Chem.* **2010**, *82*, 6321−6328.
(22) Ives, D. J. G.; Janz, G. J. *Reference Electrodes, Theory and Practice*; Academic Press: New York, 1961.
(23) Mayrhofer, K. J. J.; Strmcnik, D.; Blizanac, B. B.; Stamenkovic, V.; Arenz, M.; Markovic, N. M. *Electrochim. Acta* **2008**, *53*, 3181−3188.
(24) Paulus, U. A.; Wokaun, A.; Scherer, G. G.; Schmidt, T. J.; Stamenkovic, V.; Radmilovic, V.; Markovic, N. M.; Ross, P. N. *J Phys Chem B* **2002**, *106*, 4181−4191.
(25) Stamenkovic, V.; Schmidt, T. J.; Ross, P. N.; Markovic, N. M. *J Phys Chem B* **2002**, *106*, 11970−11979.
(26) Markovic, N.; Gasteiger, H.; Ross, P. N. *J. Electrochem. Soc.* **1997**, *144*, 1591−1597.
(27) Nørskov, J. K.; Rossmeisl, J.; Logadottir, A.; Lindqvist, L.; Kitchin, J. R.; Bligaard, T.; Jónsson, H. *J. Phys. Chem. B* **2004**, *108*, 17886−17892.
(28) Ruban, A.; Hammer, B.; Stoltze, P.; Skriver, H. L.; Nørskov, J. K. *J. Mol. Catal A: Chem.* **1997**, *115*, 421−429.
(29) Jakob, P.; Schlapka, A.; Lischka, M.; Gross, A.; Kasberger, U. *Phys. Rev. Lett.* **2003**, 91.
(30) Mavrikakis, M.; Alayoglu, S.; Nilekar, A. U.; Eichhorn, B. *Nat. Mater.* **2008**, *7*, 333−338.
(31) Sunde, S.; Ochal, P.; de la Fuente, J. L. G.; Tsypkin, M.; Seland, F.; Muthuswamy, N.; Ronning, M.; Chen, D.; Garcia, S.; Alayoglu, S.; Eichhorn, B. *J. Electroanal. Chem.* **2011**, *655*, 140−146.
(32) Marković, N. M.; Ross, P. N., Jr *Surf Sci Rep* **2002**, *45*, 117−229.